

Procoli: Profiles of cosmological likelihoods

Tanvi Karwal,^{1,*} Yashvi Patel,² Alexa Bartlett,³ Vivian Poulin,⁴ Tristan L. Smith,² and Daniel N. Pfeffer⁵

¹*Kavli Institute for Cosmological Physics, the University of Chicago, IL 60637, USA*

²*Department of Physics and Astronomy, Swarthmore College, Swarthmore, PA 19081, USA*

³*Department of Physics, University of California, Berkeley, CA 94720, USA*

⁴*Laboratoire Univers & Particules de Montpellier (LUPM),*

CNRS & Université de Montpellier (UMR-5299),

Place Eugène Bataillon, F-34095 Montpellier Cedex 05, France

⁵*Independent Researcher*

Frequentist profile likelihoods have seen a resurgence in cosmology, offering an alternative to Bayesian methods as they can circumvent the impact of prior-volume effects. This paper presents Procoli, a fast and accessible package to obtain profile likelihoods in cosmology, available on GitHub and PyPI. Procoli seamlessly integrates with MontePython, incorporating all its available data likelihoods, as well as any modified versions of CLASS. This paper provides a comprehensive overview of the Procoli code, detailing the simulated-annealing optimizer at its core and the sequential computation of the profile. As an example, we use the early dark energy model which is afflicted by prior-volume effects to illustrate the code's features. We validate its optimizer with mock data, and compare optimization techniques for both the global minimum and the profile. Procoli further enables splitting profiles into their component contributions from individual experiments, offering nuanced insights into the data and model. As a valuable addition to the cosmologist's toolkit, Procoli supplements existing Bayesian codes, contributing to more robust parameter constraints in cosmological studies.

I. INTRODUCTION

Over the last several years, cosmology has relied on Bayesian statistics for constraining models and parameters with data [1, 2]. This approach explores the data likelihood \mathcal{L} over model parameter space via Bayes theorem, determining the parameter posterior distributions \mathcal{P}

$$\mathcal{P}(\boldsymbol{\theta}|\mathbf{d}) = \frac{\Pi(\boldsymbol{\theta})\mathcal{L}(\mathbf{d}|\boldsymbol{\theta})}{\mathcal{E}(\mathbf{d})}, \quad (1)$$

as a product of the prior probability distribution Π of input model parameters $\boldsymbol{\theta}$ and the likelihood \mathcal{L} of the data \mathbf{d} given the model parameters. The evidence $\mathcal{E}(\mathbf{d})$ of the observations is usually treated as a normalization constant and ignored. Any posteriors \mathcal{P} obtained from Bayesian methods then implicitly depend on the priors Π , making this a powerful approach to incorporate expectations for and prior knowledge of $\boldsymbol{\theta}$, but they may not encapsulate ignorance of $\boldsymbol{\theta}$ well (see Jeffreys priors [3] for an attempt). Even flat priors on $\boldsymbol{\theta}$ can be subjective and informative, as they are flat priors in a chosen basis [4, 5]. They are hence non-uniform and indeed informative priors in a different basis, or a different parameterization.

For models that have priors that do not strongly influence the posteriors, posteriors resemble the data likelihood itself. This for example is the case for the standard Λ CDM model of cosmology, whose parameters have Gaussian posteriors that are well-constrained within

broad, uninformative, flat priors, across multiple parameterizations (eg. using $\ln 10^{10} A_s$ vs A_s) and the Bayesian and frequentist approaches agree [6].

The phenomenological Λ CDM model has provided a good fit to numerous data sets across several redshifts and physical scales [7–9] until recently. Lately, notable tensions and anomalies have emerged between different cosmological data sets, including the Hubble and weak-lensing S_8 tensions [10–17]. This, coupled with the phenomenological nature of Λ CDM motivates the search for physics beyond the standard Λ CDM model.

Such models are often parameterized by capturing the departure from Λ CDM via a single parameter (f below), with additional parameters describing the properties of the newly added physics. Ultimately this means that as f goes to its Λ CDM limit, the prior volume balloons because varying the other new-physics parameters no longer impacts observations and leaves the likelihood unchanged. This leads to a posterior distribution which has a strong dependence on the choice of priors [6, 18, 19].

Bayesian statistics are known to be susceptible to prior-volume effects [19, 20]. As more beyond- Λ CDM models are explored, it is prudent to develop alternative techniques to constrain models that specifically mitigate prior-volume effects. One such method is profile likelihoods, a frequentist approach with a long history of use in cosmology as well as other fields including experimental particle physics [4, 6, 20–23]. Frequentist statistics do not rely on priors, eliminating prior-volume effects in this framework. While both approaches provide parameter constraints, frequentist confidence intervals fundamentally differ from Bayesian credible intervals [4]. Results from a profile likelihood are statements about the likelihood $\mathcal{L}(\mathbf{d}|\boldsymbol{\theta})$, while Bayesian intervals are statements

* karwal@uchicago.edu

about the posterior $\mathcal{P}(\boldsymbol{\theta}|\mathbf{d})$. A 1D profile likelihood on the parameter θ_i directly traces \mathcal{L} and maximizes it at each point θ'_i in parameter space as

$$\mathcal{L}(\theta_i) = \max \mathcal{L}(\boldsymbol{\theta}|\theta_i = \theta'_i), \quad (2)$$

where the maximization is over all parameters $\theta_{j \neq i} \in \boldsymbol{\theta}$. This can then be generalized to higher dimensions for 2D, 3D and so on profiles of the likelihood. A notable advantage of this approach is the invariance of profile likelihoods under parameter redefinitions, as the likelihood remains constant regardless of whether a linear or logarithmic parameter is used (eg. A_s vs. $\ln 10^{10} A_s$), or even if an alternative parameter is used (eg. θ_* vs. H_0). The result is a curve of the effective $\chi^2 = -2 \log \mathcal{L}$ of the data vs. the profile likelihood parameter θ_i . Parameter confidence intervals can be built from this using various constructions that become equivalent in the typical case of Gaussian measurement errors far away from the physical boundaries of a parameter. The Neyman construction [24], for a single parameter, is the most straightforward: a $\Delta\chi^2 = 1$ relative to the global minimum χ^2_{\min} denotes the 1σ (68%) region, $\Delta\chi^2 = 4$ is the 2σ (95%) and so on. Interestingly, this construction does not rely on the profile itself actually being Gaussian (i.e. a parabolic χ^2 curve). It is enough that there exists a parameter redefinition in which the profile becomes Gaussian. For the remainder of this paper, we will assume this to be the case. It can also be easily generalized for N-dimensional profiles by computing the (complementary of the) cumulative of the χ^2 distribution P for $N_{\text{d.o.f.}}$, $P_{N_{\text{d.o.f.}}}(\chi^2 \geq \Delta\chi^2)$. For more complicated cases, one may rely alternatively on the Feldman-Cousins construction [4]. See Refs. [6, 19] for a concrete example in cosmology.

Over the last few years, profile likelihoods have regained favor in cosmology, owing to the popularity of several beyond- Λ CDM models that experience prior-volume effects, including models of neutrinos [6, 20–22], dark matter [25–28], and early dark energy [18, 19], several of these proposed as solutions to the Hubble tension. Investigating these models via Bayesian techniques can bias results, but deploying profile likelihoods can become computationally expensive. In this methodology paper, we present a quick and easy publicly available tool to obtain profile likelihoods in cosmology called Procoli¹. Procoli wraps MontePython [29, 30], a public sampler for cosmological data, automatically including all the data likelihoods available with MontePython. The cosmological back-end for calculating observables is assumed to be the CLASS Boltzmann code [31]. Although we present this tool wrapping MontePython, the same principles can also be immediately applied to Cobaya [32, 33], another public sampler in cosmology that wraps both the two most used Boltzmann codes CAMB [34, 35] and CLASS. The Cobaya version of our code is still in development, but

available for use upon request. We also welcome collaboration on this or any other front of further developing Procoli.

This paper is structured as follows. In Section II, we describe the Procoli code. Specifically, we describe our simulated-annealing optimizer at the heart of the profile-likelihood approach in II A, the sequential progression of this optimizer to calculate the profile in II B, and how to run Procoli and its parameters and inputs in II C. Then, using early dark energy and Λ CDM as examples, we show comparisons and features of the code in Section III, including validating the global optimizer in III A, comparing simulated annealing to a deterministic quasi-Newton optimizer in III B, and splitting profiles over the experiments they fit to in III C. Finally, we summarize and look ahead in Section IV.

II. THE PROCOLI CODE

A. Optimizer

Profile likelihoods are principally based on optimizers. At every point in parameter space, or for our purposes, at every point of parameter θ_i for which a profile is desired, the likelihood function \mathcal{L} must be optimized over all other parameters $\theta_{j \neq i} \in \boldsymbol{\theta}$. Hence, an efficient and accurate optimizer is at the core of our profile likelihood code. We employ a simulated-annealing algorithm [36] to find the maximum likelihood at each point, a scheme that is rapidly becoming the industry standard for profile-likelihood studies in cosmology [19, 22, 25, 37, 38].

Simulated annealing (SA) is a stochastic method that modifies a Metropolis-Hastings (MH) MCMC algorithm by introducing a “temperature” T to the likelihood, and changing the step size δ of the sampler in accordance [36]. Conventionally, at low temperatures, any gradients in the likelihood are enhanced, encouraging the stochastic MCMC algorithm to converge to the maximum likelihood. Practically, this works as follows. MCMCs [1] randomly take “steps” in parameter space, that is, they perturb the input parameters, calculate the observables, compare those to data, and either accept this new step, moving their position, or reject the new step, remaining at the current position in parameter space. Vanilla MH is the algorithm underlying most MCMC codes [29, 30, 32], and it decides whether to accept or reject the step based on their likelihoods as follows:

```

if  $\mathcal{L}_{\text{new}} \geq \mathcal{L}_{\text{old}}$  then
  accept
else
  draw a random number  $x \in [0, 1]$  from a uniform distribution
  if  $x < \mathcal{L}_{\text{new}}/\mathcal{L}_{\text{old}}$  then
    accept
  else
    reject

```

¹ Procoli is available via [GitHub](#) as well as [PyPI](#)

end if
end if

Modifying this, SA tempers the acceptance algorithm by exponentiating the likelihood ratio in the case of $\mathcal{L}_{\text{new}}/\mathcal{L}_{\text{old}} < 1$ usually with a temperature $T < 1$:

if $x < (\mathcal{L}_{\text{new}}/\mathcal{L}_{\text{old}})^{1/T}$ then
accept
else
reject
end if

For MH, $T = 1$. As T is decreased, features in the likelihood are sharpened, such that the probability to reject points that lower the likelihood increases with smaller T .

Besides tempering the likelihood, SA also modifies the step size or jumping factor δ of the sampler, which dictates how large a step $\Delta\theta_j$ is taken in each parameter per iteration in conjunction with the covariance matrix Σ as

$$\Delta\theta_j \simeq \delta \sqrt{\Sigma_{jj}}. \quad (3)$$

For MH, the recommended jumping factor hovers around $\delta = 2.4$ [39] (unless this is adaptively updated [30]). However, assuming we are close to the maximum likelihood, as T decreases and the likelihood is sharpened, a large step size will drastically reduce the acceptance rate. In this scenario, most proposals will be rejected as they worsen the current likelihood, stepping too far away from the maximum likelihood. Therefore, as the temperature of the likelihood is decreased, the jumping factor must also decrease. Usually, SA algorithms attempt to vary T and δ such that the acceptance rate is roughly constant [37].

In Procoli, we provide empirical recommendations for T and δ that balance efficiency and accuracy, but these can also be input by the user. Ultimately, the progression of T and δ can be improved by an adaptive algorithm which we leave to future updates to the code.

We find that an SA optimizer implemented as described above substantially improves over Minuit² [40, 41], a quasi-Newtonian optimizer often used with MontePython [6], which is deterministic in nature. The stochastic approach of SA can help the optimizer escape local minima, leading to more robust outcomes as shown in Sec. III B. An additional advantage of this approach is that it wraps an MCMC, for which one usually activates multiple parallel chains at once. Under SA, each chain effectively provides a semi-independent optimization run, and the final minimum χ^2 is chosen as the minimum of the minima of each chain, making the result more stable. We explore the differences between the two optimizers Minuit and our SA algorithm in Sections III A and III B.

B. Initialization

Most optimization methods, including SA, require an initial point to begin from. Moreover, as Procoli piggybacks over an MCMC to explore the parameter space, converging to a maximum \mathcal{L} (or minimum χ^2) is substantially faster and more accurate with an input covariance matrix Σ . Both of these requirements are easily fulfilled by initializing the profile likelihood run with a converged MCMC. This provides a maximum a posteriori (MAP) in the form of the global maximum likelihood found by the MCMC, as well as a covariance matrix for the parameter space. The convergence criteria for these input MCMC chains is not very strict, a Gelman-Rubin criteria of $R - 1 < 0.2$ suffices. Alternatively, supplying just an input covariance matrix and MAP also fulfills these requirements.

Using these, the code first finds the global best fit by starting from the MAP and using the covariance matrix, carrying out an SA optimization as described above. The recommendations for T and δ for the global optimizer are more thorough, as parameter confidence intervals from profile likelihoods are found at $\Delta\chi^2 = 1$ relative to the global minimum χ_{min}^2 .

Once this global minimum is determined, the code takes iterative steps away from this minimum along either direction in the profile likelihood parameter θ_i , at a user-defined step-size $\Delta\theta_i$. That is, after the global best fit $\theta_{\text{min}} = \theta^0$ is found, the code fixes

$$\theta_i = \theta_i^{+1} \equiv \theta_{i,\text{min}} + \Delta\theta_i. \quad (4)$$

The superscripts denote the iteration, with 0 corresponding to the global minimum χ^2 . It then initializes the SA optimizer providing θ^0 as initial value for all other parameters $\theta_{j \neq i}$, and the covariance matrix Σ from the MCMC run. The optimizer finds a new minimum θ^{+1} , which becomes the input for the next iteration. This sequence continues, with each iteration fixing

$$\begin{aligned} \theta_i &= \theta_i^{+n} \equiv \theta_i^0 + n\Delta\theta_i \\ \theta_{j \neq i} &\in \theta^{+(n-1)}. \end{aligned} \quad (5)$$

A similar sequence progresses in the negative direction for θ_i^{-n} and θ^{-n} , continuing till the user-defined ranges for exploration in θ_i are saturated, resulting in a sequence of optimized points $\{\theta^{-N}, \dots, \theta^{-1}, \theta^0, \theta^{+1}, \dots, \theta^{+M}\}$. Note that $N \neq M$ usually, as the global best fit θ^0 may be closer to one bound.

For this sequential profile likelihood of θ_i , we recommend that the first jumping factor δ in the SA optimizer be $\delta \leq \Delta\theta_i/\sigma_i$, where σ_i is the 1σ error on the likelihood-profile parameter θ_i from the covariance matrix. This avoids scenarios where the optimizer might overshoot the next minimum, and instead allows the optimizer to converge to this minimum.

This procedure records not only the profile likelihood, but also the values of all input and derived parameters across the profile, including a breakdown of χ^2 per experiment.

² Minuit is publicly available through PyPI.

C. Implementation

The optimization method and sequential calculation of the likelihood profile described above are implemented by Procoli in Python. The Procoli Python package relies primarily on MontePython to perform the SA optimization via running MCMCs through subprocesses, and to analyze the chains produced to find the best fit and calculate the covariance matrix. It also uses functions defined in GetDist [42] to check any provided MCMC chains and their convergence, but this is not necessary as the user can alternatively provide just a covariance matrix and a starting guess for the global best fit. The code then takes as input:

- **chains_dir**: path to the directory for the location of the MCMC chain files or alternatively, the covariance matrix (`.covmat`) and best-fit guess (`.bestfit`) files, in the format used by MontePython. This directory must also contain a `log.param` file that includes the experiments, and cosmological and nuisance parameters to be used, identical to a usual MontePython MCMC run.
- **prof_param**: name of the profile likelihood parameter θ_i as understood by MontePython, same as in the `log.param`
- **prof_incr** increment $\Delta\theta_i$ at which to query the profile
- **prof_min** and **prof_max**: the range in θ_i to explore

Additionally, the user can also specify the number of chains to run in parallel for each optimization by setting **processes** (default assumed to be 5). This is effectively the number of MCMC chains used in the simulated annealing. A complete list of arguments is documented in the code on GitHub.

The code begins by looking for MCMC chain files or for the covariance matrix and input guess for the best fit. If only the chains are provided, it obtains the covariance matrix and best-fit guess using MontePython analysis tools. It then begins a global optimizer using any specified lists of values for the jumping factor and temperature or uses the defaults. Next, it begins the profile likelihood exploration using the input increments $\Delta\theta_i = \text{prof_incr}$, till it saturates either **prof_min** or **prof_max**. The jumping factor and temperature lists for the profile differ from those for the global best fit search, and both can be modified by the user.

At each iteration, the code populates a sub-directory within the parent directory with the MCMC chains run by the optimizer. These chains are overwritten per iteration $\Delta\theta_i$ to save memory space. A text file in the parent directory keeps track of the likelihood profile and the location of the run. If prematurely terminated, the code restarts the profile at the next point after the last complete iteration. Users can keep track of how long

each iteration takes, and therefore how long the entire run would take via handy time-stamp files produced.

Examples for a complete session are recorded on the GitHub, using Jupyter notebooks as well as a python script that can be submitted to a cluster. Procoli also includes several useful plotting and analysis functions, which are illustrated in these Jupyter notebooks.

III. EXAMPLES AND FEATURES

For the purposes of demonstrating the code, we explore two cosmological models, Λ CDM and early dark energy (EDE) [43–47]. EDE adds an additional component to base Λ CDM that behaves like a cosmological constant at early times, then close to matter-radiation equality, rapidly dilutes away, such that its impact on cosmology is localized in redshift. It was originally proposed as a solution to the Hubble tension [10, 11, 47], as it shifts the CMB-predicted H_0 into agreement with local distance-ladder measurements [12, 48]. The CMB predicts H_0 via a very precise measurement of the angular size θ_* of the sound horizon r_s at the surface of last scatter [43, 46, 47, 49–51]. Approximately, $\theta_* \propto H_0 r_s$. The addition of EDE makes the pre-recombination universe expand slightly faster, shrinking r_s , which increases H_0 to fix the observed value of θ_* .

Numerous models can produce the EDE phenomenology [45, 52–62]. Here we concentrate on ultra-light-axions-inspired EDE, using AxiCLASS³ [44, 45]. The parameters of this model are the maximum fractional energy density f_{ede} in EDE, the redshift z_c (or alternatively the scale factor a_c) at which EDE density peaks, and the initial value ϕ_i of the scalar field that forms EDE⁴. As $f_{\text{ede}} \rightarrow 0$, the properties of this negligible component defined by z_c and ϕ_i become unconstrained. Then, the choice of uniform priors in $\log_{10} z_c$ and ϕ_i become informative priors, rapidly growing the prior volume in the direction $f_{\text{ede}} \rightarrow 0$ and biasing Bayesian posteriors as shown in Fig. 1.

Besides the EDE parameters, we also vary the six Λ CDM parameters: the physical densities of cold dark matter ω_c and baryons ω_b , the amplitude A_s and tilt n_s of the primordial power spectrum, the optical depth τ_{reio} to reionization and the Hubble expansion rate H_0 today.

Our primary example fits an EDE cosmology to the Planck 2018 CMB spectrum including the low- ℓ TT and EE data and the high- ℓ TTTEEE data [63]. Some of our demonstrations additionally include the Planck CMB lensing spectrum [64], supernova data from Pantheon [9], as well as BAO data from BOSS DR12 [8], 6dF [65] and SDSS MGS [66]. Beyond these, any likelihoods available in MontePython can be readily used in Procoli.

³ AxiCLASS is publicly available on GitHub

⁴ Usually, this parameter is denoted by θ_i , but we use ϕ_i here to distinguish it from the discussion in Sec. II

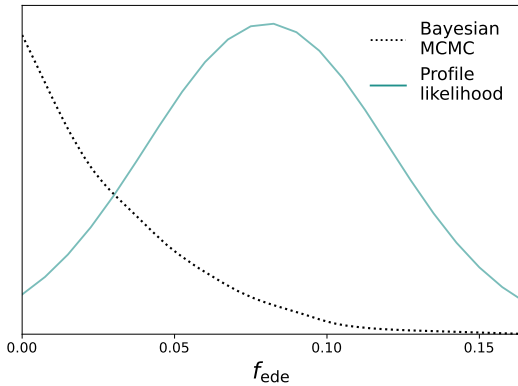


FIG. 1. Bayesian posteriors on the amount f_{ede} of EDE are shown (dotted black) alongside a likelihood profile (solid green) on the same parameter, using the same data sets, namely Planck CMB primaries. EDE posteriors from Bayesian MCMCs are impacted by prior volume growing in the direction of $f_{\text{ede}} \rightarrow 0$, biasing constraints towards $f_{\text{ede}} = 0$, despite the maximum likelihood being closer to $f_{\text{ede}} \simeq 0.07$ as seen from the maximum of the solid blue curve.

With this setup, we perform several tests to check the robustness of our code, and to provide recommendations for usage. Specifically, in the following, we demonstrate the accuracy of the global optimizer with an example using mock data generated for an EDE cosmology in III A. We next compare our optimizer to simply binning the MCMC chains and looking for the MAP within bins, and to using Minuit, a deterministic optimizer for the profile in III B. Besides these tests, we also showcase a key feature of Procoli in III C - extracting the χ^2 per experiment, which can provide deeper insights into data with profile likelihoods.

A. Accuracy of the global best fit

To validate the global optimizer, we generated noiseless mock CMB data up to multipole $\ell = 3000$ in a fiducial EDE cosmology using the parameters shown in Table I. Then, using the default settings for the SA optimizer in Procoli, we find a global best fit for this mock data. Two different inputs are tested for the initial best-fit guess and covariance matrix. One from an EDE fit to just Planck data, with an initial guess that has $\chi^2 = 592$ for the mock data. The second input is taken from an EDE fit to Planck CMB, Pantheon supernovae, BAO and SH0ES data, with a comparatively worse $\chi^2 = 1163$ for the mock data. Although these are not optimal inputs as they are based on different data, this setup provides a useful test case to validate the optimizer searching for the global best fit. Doing so, we nearly exactly recover the true cosmology and find $\chi^2_{\text{min}} = 0.00054$ in the case of the smaller input χ^2 and $\chi^2_{\text{min}} = 0.00087$ for the second case, with differences of $\Delta\chi^2 < 0.001$ between the two

scenarios. Hence, even with sub-optimal inputs, the SA optimizer is excellent at recovering the true parameter values.

These scenarios effectively stress-test the SA optimizer. Usually, global optimizers are initialized from an MCMC run on the same data sets, providing better input MAPs and covariance matrices, scenarios which are only expected to improve on the performance above. For the sake of comparison, a quasi-Newtonian optimizer subjected to the same atypical scenario above could not recover the true inputs. We test Minuit under the same conditions, with the same sub-optimal guesses for the initial point and covariance matrix and it recovers $\chi^2_{\text{min}} = 255.86$ and $\chi^2_{\text{min}} = 266.71$ respectively in the two cases. Here, we use the `iminuit.minimize` function as a swap for `scipy.optimize.minimize` in MontePython, as these have the same interface, although this does not allow utilization of the full functionality of Minuit. Also note that this is not usually how Minuit is employed to optimize - relying on an input covariance matrix and starting guess for the best fit that were not generated for the data set in question. We simply highlight that Minuit is more sensitive to the initial guess and these unusual conditions form a critical impediment to it, unlike SA whose stochasticity can overcome a bad initial starting point. Beyond profile likelihoods, we recommend the use of SA optimizers for maximum-likelihood searches with real CMB data, which is far noisier and higher-dimensional than this test case. The stochasticity of SA optimizers leads to more robust best fits than deterministic algorithms like quasi-Newton methods.

In Fig. 2, we show a global optimizer run for an EDE cosmology with real data, namely Planck CMB primaries. For this, we use the default settings in Procoli for the jumping factor and temperature progression over the SA optimization, as labeled on the figure. By default, each chain for each step in the SA ladder takes $N = 4000$ MCMC steps, including rejected steps, but here we run the optimizer slightly longer with $N = 5000$. For each SA step, multiple chains are run in parallel to explore the parameter space, further capitalizing on the stochastic nature of SA. Then, the best-fit point of all previous SA steps across all chains is used as input for the next SA step. As each step has a finite jumping factor δ , the optimizer can still escape local minima. As the temperatures T and jumping factors are slowly lowered, the differences in the χ^2 of chains follow suit. Ultimately, the optimizer finds the maximum global likelihood with multiple chains. EDE and Λ CDM parameter values per MCMC step are shown in Appendix A.

We again compare the results for a global best fit found using Minuit to our SA optimizer, and find that Minuit results in only a slightly worse fit by $\Delta\chi^2_{\text{min}} = 0.89$. Minuit performs far better in this case when its inputs are generated for the data set in question, the usual scenario in which Minuit is run post an MCMC. However, for profile likelihoods that set the 1σ parameter limits at $\Delta\chi^2 = 1$, this difference in χ^2 is substantial, making SA

Parameter	Fiducial value	Input MAP	$\Delta\theta_i^{\text{input}}/\theta_i^{\text{fid}}$	SA best fit	$\Delta\theta_i^{\text{SA}}/\theta_i^{\text{fid}}$	Input MAP	$\Delta\theta_i^{\text{input}}/\theta_i^{\text{fid}}$	SA best fit	$\Delta\theta_i^{\text{SA}}/\theta_i^{\text{fid}}$
ω_b	0.02291	0.02262	-0.01	0.02291	0.0001	0.02275	-0.007	0.02291	-0.0001
ω_{cdm}	0.1278	0.12724	-0.004	0.12785	0.0004	0.13199	0.03	0.12777	-0.0003
h	0.7051	0.69737	-0.01	0.70532	0.0003	0.71967	0.02	0.70494	-0.0002
$\ln 10^{10} A_s$	3.049	3.06196	0.004	3.04903	1e-05	3.07104	0.007	3.04879	-7e-05
n_s	0.9771	0.98001	0.003	0.97726	0.0002	0.99013	0.01	0.97696	-0.0001
τ_{reio}	0.0593	0.05674	-0.04	0.05929	-9e-05	0.05714	-0.04	0.05924	-0.001
f_{ede}	0.1173	0.07319	-0.4	0.11781	0.004	0.12271	0.05	0.11691	-0.003
$\log_{10} a_c$	-3.614	-3.57397	-0.01	-3.61403	9e-06	-3.56097	-0.01	-3.61293	-0.0003
ϕ_i	2.689	2.72609	0.01	2.68889	-4e-05	2.76404	0.03	2.68805	-0.0004
χ^2		591.83		0.00054		1162.78		0.00087	

TABLE I. The parameters of the fiducial cosmology used to generate the mock data are compared to the parameters found in the global best fit using the Procoli default SA optimizer. We also show relative differences $(\theta_i - \theta_i^{\text{fid}})/\theta_i^{\text{fid}}$ for each column. SA best fits from two different starting points are shown - the first input MAP comes from an EDE fit to Planck data, with its distance from the true best-fit fiducial value captured by its χ^2 for the mock data in the last row. The second input MAP comes from an EDE fit to Planck CMB + Pantheon supernovae + BAO + SH0ES data, a substantially worse starting guess as seen from its χ^2 for the mock data. Each of these input MAPs are followed by their best fits found through the SA optimizer.

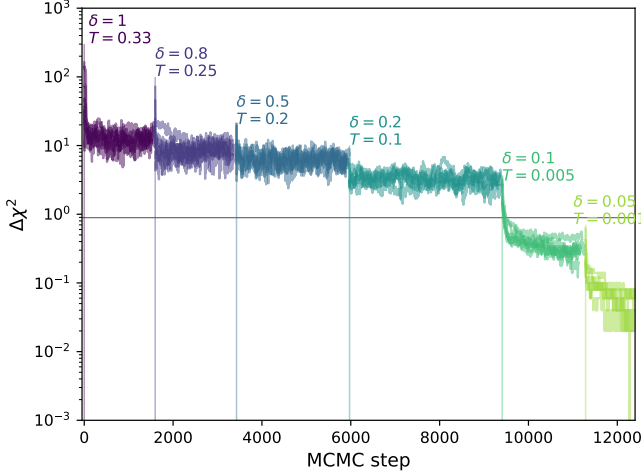


FIG. 2. The $\Delta\chi^2$ relative to the minimum $\chi_{\text{min}}^2 = 2761.3$ for a global optimizer run using the default settings in Procoli for the jumping factor δ and temperature T for the SA ladder. We separate the steps by color and vertical lines and denote the values of δ and T used. Each chain at each step in the ladder took a total of 5000 MCMC steps, including the rejected steps. The horizontal line marks the minimum global χ^2 achieved by Minuit, $\Delta\chi_{\text{min}}^2 = 0.89$ greater than the Procoli minimum. The run was for an EDE cosmology constrained by Planck CMB primaries.

optimizers the superior choice.

B. Comparison with Minuit and binned MCMC

Beyond just the global best fits, the SA and quasi-Newtonian optimizers can also be compared on the full profile likelihoods, as we do in Fig. 3. Alongside, we also compare simply binning the points sampled by an MCMC in narrow bins centered at the same $\Delta\theta_i$ increments as the profile likelihoods, picking the MAP per

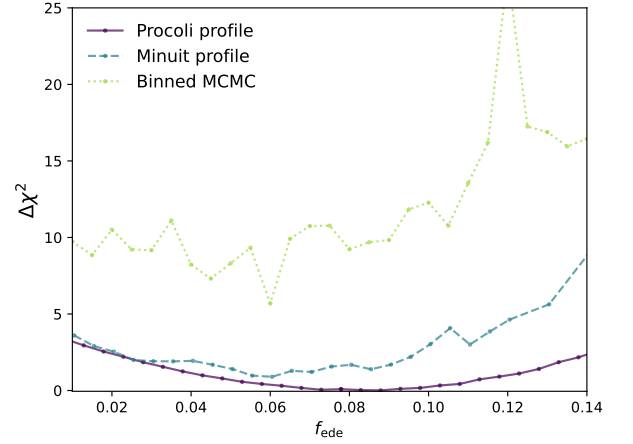


FIG. 3. Profile likelihoods of Planck CMB primaries for f_{ede} obtained via three approaches are compared. For solid purple, we use Procoli to produce a profile likelihood, using its SA optimizer. For dashed blue, we use the same sequential approach described in Section II B, but use Minuit instead of SA. In dotted green, we bin the samples from a vanilla Metropolis-Hastings MCMC in narrow bins centered at a given f_{ede} , picking the MAP per bin. To rescale them and aid visuals, we subtract out the minimum $\chi^2 = 2761.21$ found across all three profile from each curve.

bin.

The profile based on a Metropolis-Hastings MCMC is mildly biased towards lower f_{ede} , partly due to being afflicted by prior volume effects. Moreover, the profile is extremely jagged and the MAPs in each bin are > 4 in χ^2 away from the minima found by Procoli. Basing a profile likelihood on simply binning MCMC posteriors can not only be misleading, but may also completely miss the true minimum, as is the case for the global MAP of the full MCMC chains. In particular, the global MAP finds

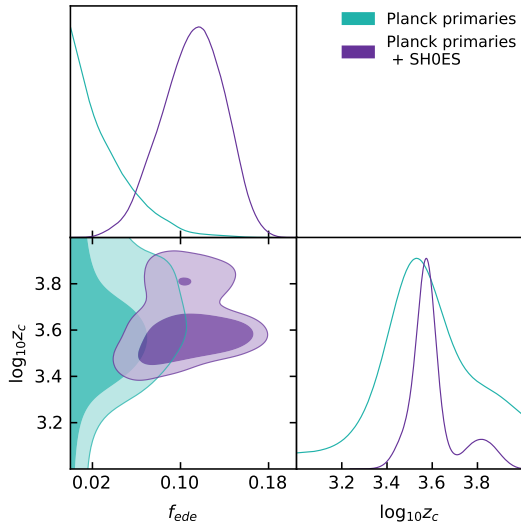


FIG. 4. Any bimodality in z_c is very mild when EDE is constrained with just Planck CMB primaries, indeed the two modes are connected within the 1σ posterior contour as shown by the green contours. The bimodality is sharpened and more clearly visible with the inclusion of the local H_0 measurement [67] in the purple contours.

$\log_{10} z_c = 3.82$, while the global best fit found by Procoli as described in Sec. III A finds $\log_{10} z_c = 3.57$. This arises from a mild bimodality in EDE cosmologies in the injection redshift z_c of EDE, shown in Fig. 4, which is recovered by a standard MH MCMC that converges within finite time. The bimodality also forms an additional factor biasing the binned MCMC curve in Fig. 3 towards lower f_{ede} .

Using the deterministic optimizer Minuit, we also perform the same sequential search for the likelihood profile as described in Sec. II B, but swapping the SA optimizer for Minuit. The same chains as the binned MCMC curve are used for input for this curve, i.e. Minuit is initialized at a MAP that tracks the higher- z_c mode, instead of the lower- z_c mode which covers the true global best fit. Although this setup performs far better than a binned MCMC, it does not escape the high- z_c local minimum which it tracks for all f_{ede} , failing to find the true best fit. A similar profile is recovered by Procoli if z_c is restricted to this mode with $\log_{10} z_c > 3.7$ as shown in Fig. 5.

Finally, with the same inputs as the binned MCMC and the Minuit curves, the SA optimiser in Procoli finds the true best fit in the lower- z_c mode. Its stochastic approach is able to overcome the mild bimodality of EDE. Moreover, it finds a smoother profile with consistently lower χ^2 values.

This example with EDE does not generalize divergent results from quasi-Newtonian and SA optimizers. It simply highlights the possible pitfalls of deterministic optimizers when employed over a complex and high-dimensional parameter space and urges caution when us-

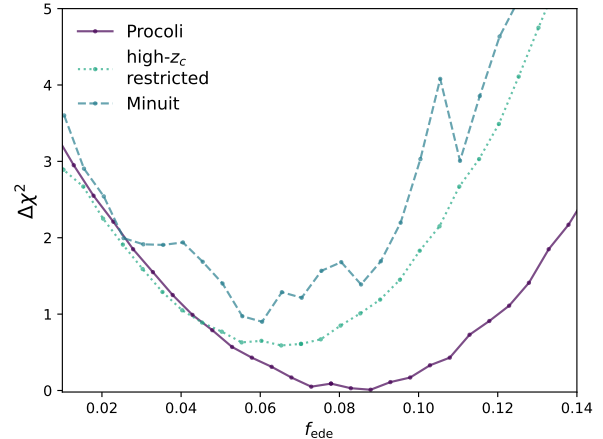


FIG. 5. We compare the profile likelihoods of Planck CMB primaries for f_{ede} obtained using two different optimizers - SA via Procoli and a quasi-Newton method via Minuit. Minuit (dashed blue) gets stuck in a local minimum with EDE injection redshift $\log_{10} z_c > 3.7$, which is not the true global minimum. Procoli (solid purple) finds a better minimum at $\log_{10} z_c < 3.7$, but a profile resembling the Minuit profile can be recovered by Procoli by restricting it to this high- z_c mode (dotted green). The solid purple Procoli curve and the dashed blue Minuit curves are the same as in Fig. 3.

ing them to produce likelihood profiles.

C. Differentiating χ^2 per experiment

For each point in the likelihood profiles produced by Procoli, the code also calculates the χ^2 for each experiment listed in the `log.param`. This can provide powerful insights into which experiments are driving constraints and also automatically allows the user to produce profiles using a subset of experiments as shown in Fig. 6.

For demonstrating this, we profile H_0 in a Λ CDM model constrained by Planck CMB, BAO and Pantheon supernova data. The left panel of Fig. 6 shows the profiles for these three data sets and their cumulative total χ^2 , with each curve rescaled by subtracting out the minimum χ^2 for that specific curve. This $\chi^2 - \chi^2_{\text{min}}$ exactly quantifies the contribution of each data set to the combined profile likelihood, as shown by the solid black curve balancing the individual profiles of BAO and Planck CMB data. It is also immediately clear which datasets are most constraining for the profile parameter (Planck CMB), and the one with minimal impact to the profile (Pantheon supernovae). While this is no surprise for the thoroughly studied Λ CDM model, such splits differentiating the χ^2 each experiment contributes to likelihood profiles can provide valuable insights into more complicated models.

For the left panel in Fig. 6, we combined individual CMB likelihoods under Planck CMB, but these can

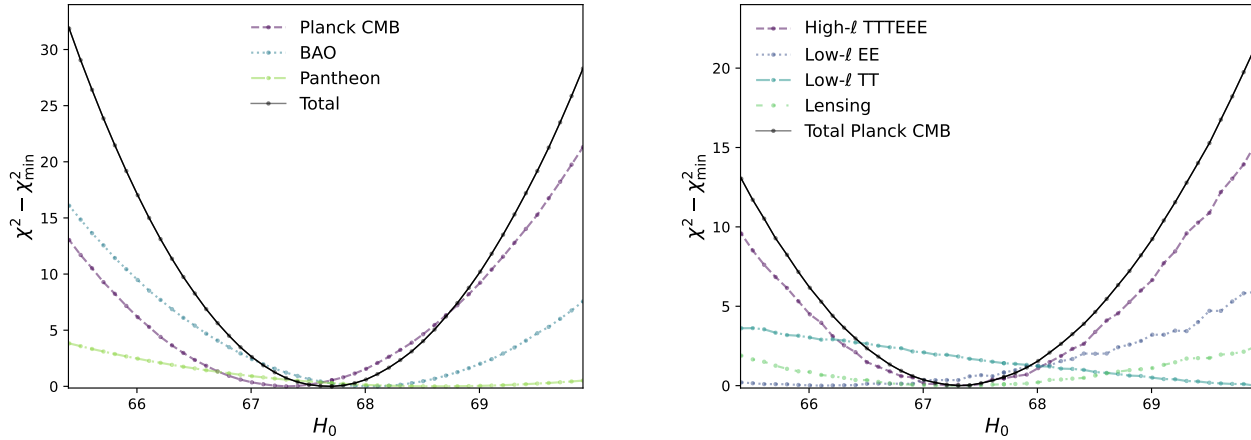


FIG. 6. A breakdown of the χ^2 per experiment for a profile likelihood on H_0 in Λ CDM, fitting to the experiments listed. For each curve, we subtract out its minimum χ^2 to show them on the same scale. *Left:* The full Planck CMB dataset is shown in dashed purple, BAO in dotted blue and Pantheon supernovae in dash-dotted green. The total χ^2 shown in solid black is the quantity optimized for producing this profile. *Right:* We further breakdown the elements contributing to the Planck CMB curve on the left plot (same as solid black here), namely the high- ℓ TTTEE spectrum (dashed purple), the low- ℓ EE (dotted blue) and TT (dash-dotted teal), and the CMB lensing power spectrum (dash-dot-dotted green).

also be examined separately as in the right panel. The solid black curve in the right panel now corresponds to the combined Planck CMB likelihood, and is the same as the dashed purple curve in the left plot. For just Planck CMB data, these profiles result in a constraint $H_0 = 67.3 \pm 0.54$ km/s/Mpc, while the combined data sets from the left panel result in the slightly more stringent constraint $H_0 = 67.7 \pm 0.42$ km/s/Mpc, as expected with the addition of more data. Simply by considering just a subset of the experiments from the left panel, one can automatically produce a profile on H_0 with only Planck CMB data, effectively getting multiple profiles for the price of one.

Another notable feature is the varying level of smoothness of each curve particularly in the right panel of Fig. 6. For example, from this one can read off that the wrinkles in the low- ℓ EE data contribute the most noise to the Planck CMB profile, and any optimizations over Planck CMB data. Such χ^2 splits over experiments hence also provide insight into the data itself.

IV. CONCLUSIONS

Bayesian and frequentist statistics are two alternative approaches to parameter estimation with data. Dedicated work by cosmologists has built up a strong arsenal of Bayesian tools, powerful at incorporating prior information on model parameters. The explicit reliance on priors can however leave Bayesian approaches susceptible to prior-volume effects that bias results, including in early dark energy cosmologies, the example used in this work. As we search for new physics beyond Λ CDM and

for the true fundamental model of the Universe, it is imperative that our parameter estimations be free of bias.

Frequentist statistical tools such as profile likelihoods form a means of obtaining parameter estimates free of priors, providing a valuable supplement to Bayesian constraints. These contribute additional insight into both the data and theoretical models, with constraints that have fundamentally complementary interpretations. Bayesian constraints are statements about the posterior, while frequentist constraints constitute statements about the data likelihood. With cosmic anomalies hinting at new physics and an immense influx of high-resolution cosmological data expected in the coming years, it is crucial to build up the framework for alternative statistical approaches in cosmology.

This work presents Procoli, a straightforward and fast publicly available Python package to obtain profile likelihoods in cosmology. Procoli wraps MontePython, a sampler written for use with the CLASS Boltzmann code, automatically incorporating not only all data likelihoods available for use with MontePython, but also all modified versions of CLASS that implement physics beyond the standard Λ CDM model. Here we describe the code and demonstrate its features. Procoli calculates profile likelihoods sequentially, maximizing the likelihood at each point over the profile parameter, using the previous adjacent point to initialize the next. At their core, profile likelihoods depend on reliable optimizers. We validate the simulated-annealing optimizer used in Procoli with mock EDE data, and find it to be more robust and stable than a quasi-Newtonian method on comparison with Minuit, both for finding a global best fit and for the profile itself. Finally, we demonstrate Procoli functionality

for dissecting the χ^2 per experiment to gain additional insight into the data and the cosmological model. Besides these illustrations of Procoli, we also provide example running scripts, output of completed runs and basic plotting functionality on the GitHub.

During the final development of this code, the PROSPECT code [25] was released, another tool to extract profile likelihoods in cosmology. Both Procoli and PROSPECT use simulated-annealing optimizers, but these are implemented differently. Procoli sequentially constructs the likelihood profile and currently has a set simulated-annealing ladder of temperature and step-size progressions, to be updated to an adaptive ladder in the next version. Each point in the profile is initialized from a previously-optimized, adjacent point such that inputs to the SA optimizer are close to the maximum likelihood already. PROSPECT approaches the profile in parallel and implements an adaptive simulated-annealing algorithm. As input for each point in the profile, it takes MAPs from the MCMC chains in narrow bins, similar to those shown in Fig. 3. With frequentist profile likelihoods regaining popularity in cosmology, having multiple codes to perform similar tasks can be extremely useful both for comparison and accessibility.

Bayesian and frequentist statistical approaches each have strong advantages. Employing them in conjunction can yield deeper, unbiased insights into data as well as cosmological models and lead to a better understanding of the impact of prior choices. Procoli contributes to this goal, adding to the growing arsenal of frequentist tools at the disposal of cosmologists.

ACKNOWLEDGMENTS

We thank Marco Raveri, Cyrille Doux, Shivam Pandey, José Luis Bernal and Nils Schöneberg for discussions that helped improve this work. We additionally thank Shar Daniels for their input during the early stages of develop-

ing this code. Finally, we are grateful to Marco Gatti for contributing computing resources for the completion of this project. TK was supported by funds provided by the Kavli Institute for Cosmological Physics at the University of Chicago through an endowment from the Kavli Foundation. VP is supported by funding from the European Research Council (ERC) under the European Union’s HORIZON-ERC-2022 (grant agreement no. 101076865). VP is also supported by the European Union’s Horizon 2020 research and innovation program under the Marie Skłodowska-Curie grant agreement no. 860881-HIDDeN. TLS is supported by NSF Grant No. 2009377. The authors acknowledge the use of computational resources from the Excellence Initiative of Aix-Marseille University (A*MIDEX) of the Investissements d’Avenir program and from the LUPM’s cloud computing infrastructure founded by Ocevu labex and France-Grilles.

Appendix A: Global optimization convergence

For global optimizers, we show how Procoli explores the parameter space, converging over SA steps towards the global minimum χ^2 . Specifically in Fig. 7, we show the six Λ CDM parameters when fit to Planck CMB primaries with an EDE cosmology. The EDE parameters for this optimization are shown in Fig. 8. The corresponding progression in χ^2 is shown in the main text in Fig. 2.

Similarly, we also show the convergence of the optimizer to the fiducial cosmology for our validation tests in Figs. 9 and 10. The true values of all nine cosmological parameters are correctly identified by Procoli. Compared to the curves in Figs. 7 and 8, these curves are far more concentrated around the true input parameter values as the mock data generated was noiseless. The initial starting point is the scenario with $\chi^2 = 1162.78$ in Table I, which may be beyond the y -limits of the zoomed-in figures.

-
- [1] Antony Lewis and Sarah Bridle, “Cosmological parameters from CMB and other data: A Monte Carlo approach,” *Phys. Rev. D* **66**, 103511 (2002), [arXiv:astro-ph/0205436](#).
 - [2] Robert D. Cousins, “Why isn’t every physicist a Bayesian?” *Am. J. Phys.* **63**, 398 (1995).
 - [3] Harold Jeffreys, “An invariant form for the prior probability in estimation problems,” *Proc. R. Soc. A* **186**, 453–461 (1946).
 - [4] Gary J. Feldman and Robert D. Cousins, “A Unified approach to the classical statistical analysis of small signals,” *Phys. Rev. D* **57**, 3873–3889 (1998), [arXiv:physics/9711021](#).
 - [5] J. Colin Hill, Evan McDonough, Michael W. Toomey, and Stephon Alexander, “Early dark energy does not restore cosmological concordance,” *Phys. Rev. D* **102**, 043507 (2020), [arXiv:2003.07355 \[astro-ph.CO\]](#).
 - [6] P. A. R. Ade *et al.* (Planck), “Planck intermediate results. XVI. Profile likelihoods for cosmological parameters,” *Astron. Astrophys.* **566**, A54 (2014), [arXiv:1311.1657 \[astro-ph.CO\]](#).
 - [7] N. Aghanim *et al.* (Planck), “Planck 2018 results. VI. Cosmological parameters,” *Astron. Astrophys.* **641**, A6 (2020), [Erratum: *Astron. Astrophys.* 652, C4 (2021)], [arXiv:1807.06209 \[astro-ph.CO\]](#).
 - [8] Shadab Alam *et al.* (BOSS), “The clustering of galaxies in the completed SDSS-III Baryon Oscillation Spectroscopic Survey: cosmological analysis of the DR12 galaxy sample,” *Mon. Not. Roy. Astron. Soc.* **470**, 2617–2652 (2017), [arXiv:1607.03155 \[astro-ph.CO\]](#).
 - [9] D. M. Scolnic *et al.* (Pan-STARRS1), “The Complete Light-curve Sample of Spectroscopically Confirmed SNe

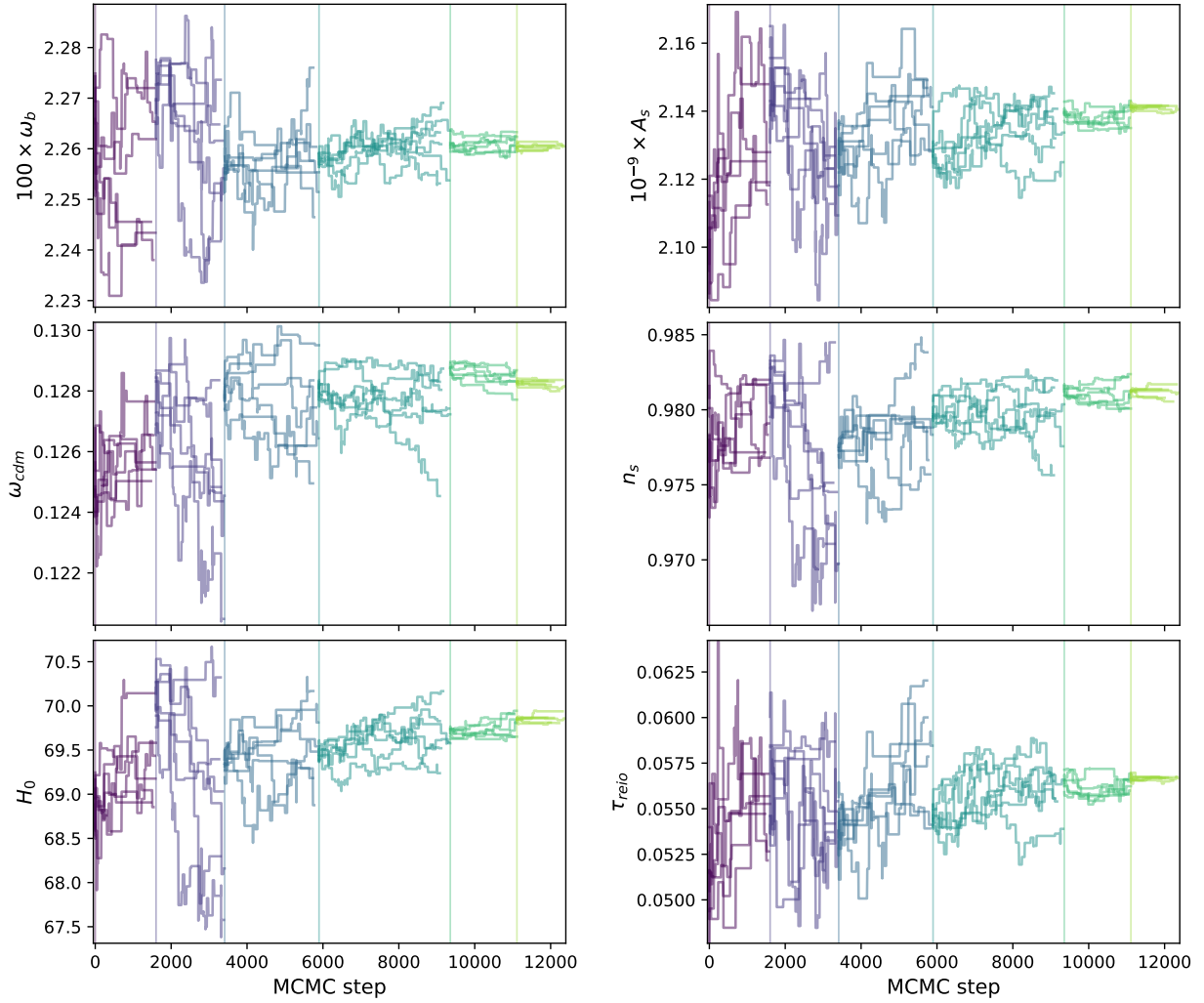


FIG. 7. Convergence of the 6 Λ CDM parameters over the global optimizer run in an EDE cosmology constrained by Planck primaries. Each step in the SA ladder is differentiated by color and by a vertical line. The figure shows the same global optimizer run as in Fig. 2, which also shows the temperature and jumping factors per SA step.

- Ia from Pan-STARRS1 and Cosmological Constraints from the Combined Pantheon Sample,” *Astrophys. J.* **859**, 101 (2018), [arXiv:1710.00845 \[astro-ph.CO\]](#).
- [10] L. Verde, T. Treu, and A. G. Riess, “Tensions between the Early and the Late Universe,” *Nature Astron.* **3**, 891 (2019), [arXiv:1907.10625 \[astro-ph.CO\]](#).
- [11] Elcio Abdalla *et al.*, “Cosmology intertwined: A review of the particle physics, astrophysics, and cosmology associated with the cosmological tensions and anomalies,” *JHEAp* **34**, 49–211 (2022), [arXiv:2203.06142 \[astro-ph.CO\]](#).
- [12] Adam G. Riess and Louise Breuval, “The Local Value of H_0 ,” (2023) [arXiv:2308.10954 \[astro-ph.CO\]](#).
- [13] Lucas F. Secco, Tanvi Karwal, Wayne Hu, and Elisabeth Krause, “Role of the Hubble scale in the weak lensing versus CMB tension,” *Phys. Rev. D* **107**, 083532 (2023), [arXiv:2209.12997 \[astro-ph.CO\]](#).
- [14] A. Amon *et al.* (DES), “Dark Energy Survey Year 3 results: Cosmology from cosmic shear and robustness to data calibration,” *Phys. Rev. D* **105**, 023514 (2022), [arXiv:2105.13543 \[astro-ph.CO\]](#).
- [15] L. F. Secco *et al.* (DES), “Dark Energy Survey Year 3 results: Cosmology from cosmic shear and robustness to modeling uncertainty,” *Phys. Rev. D* **105**, 023515 (2022), [arXiv:2105.13544 \[astro-ph.CO\]](#).
- [16] Shun-Sheng Li *et al.*, “KiDS-1000: Cosmology with improved cosmic shear measurements,” *Astron. Astrophys.* **679**, A133 (2023), [arXiv:2306.11124 \[astro-ph.CO\]](#).
- [17] Roohi Dalal *et al.*, “Hyper Suprime-Cam Year 3 results: Cosmology from cosmic shear power spectra,” *Phys. Rev. D* **108**, 123519 (2023), [arXiv:2304.00701 \[astro-ph.CO\]](#).
- [18] Tristan L. Smith, Vivian Poulin, José Luis Bernal, Kimberly K. Boddy, Marc Kamionkowski, and Riccardo Murgia, “Early dark energy is not excluded by current large-scale structure data,” *Phys. Rev. D* **103**, 123542 (2021), [arXiv:2009.10740 \[astro-ph.CO\]](#).
- [19] Laura Herold, Elisa G. M. Ferreira, and Eiichiro Komatsu, “New Constraint on Early Dark Energy from Planck and BOSS Data Using the Profile Likelihood,” *Astrophys. J. Lett.* **929**, L16 (2022), [arXiv:2112.12140](#)

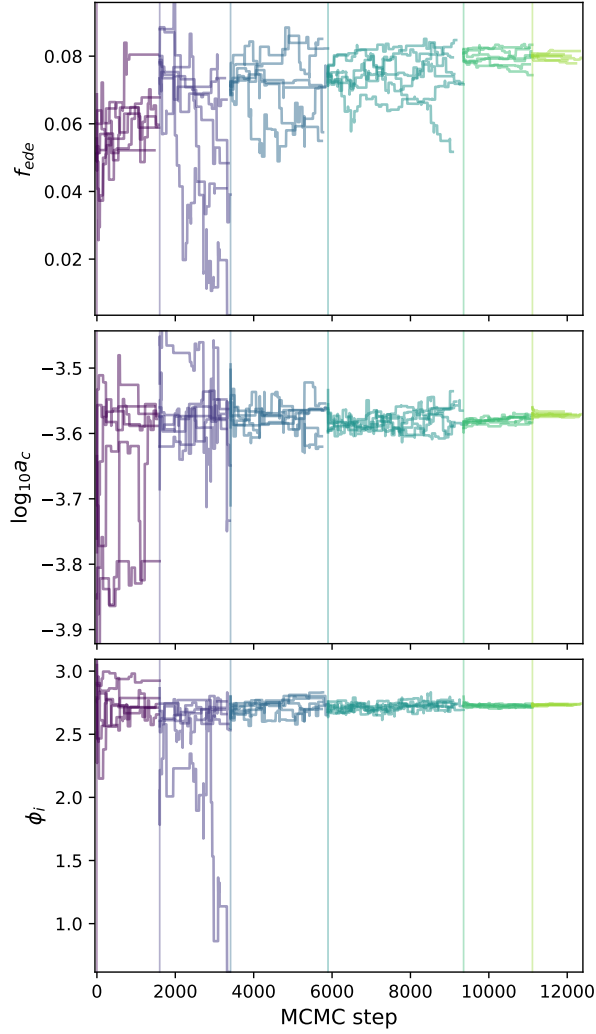


FIG. 8. Convergence of EDE parameters over the same global optimizer run as in Figs. 2 and 7. Each step in the SA ladder is differentiated by color and by a vertical line. The EDE parameters are the amount f_{ede} of EDE, the injection scale factor $\log_{10} a_c$ and the initial value ϕ_i of the scalar field.

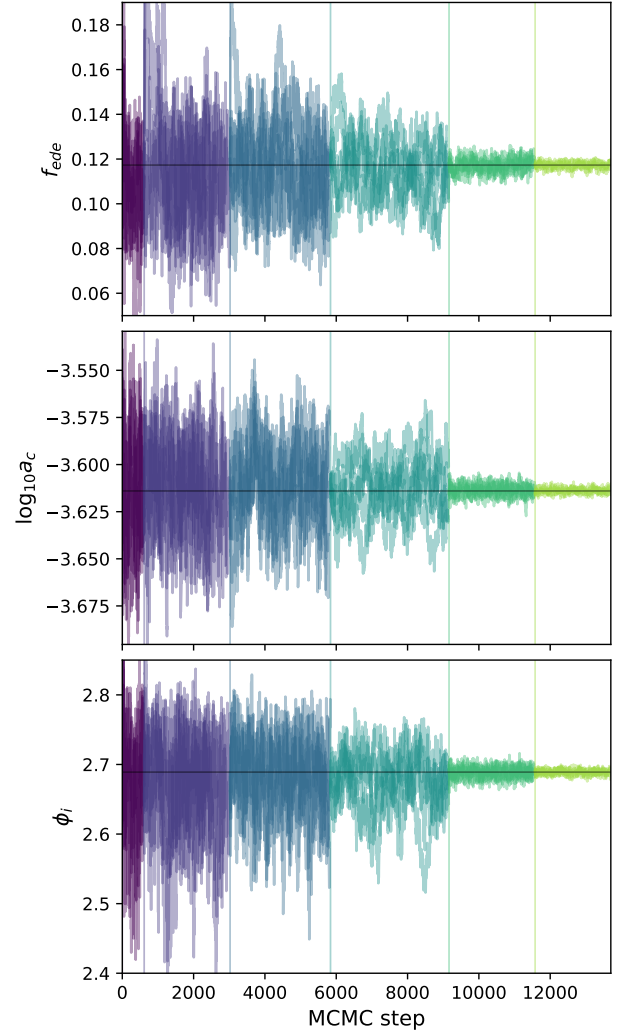


FIG. 9. Convergence of EDE parameters to the fiducial cosmology in Table I, using Procoli default settings for the global optimization. Each step in the SA ladder is differentiated by color and by a vertical line. The horizontal black lines mark the positions of the input fiducial cosmology.

- [astro-ph.CO].
- [20] Jan Hamann, “Evidence for extra radiation? Profile likelihood versus Bayesian posterior,” *JCAP* **03**, 021 (2012), [arXiv:1110.4271 \[astro-ph.CO\]](#).
- [21] Nathalie Palanque-Delabrouille, Christophe Yèche, Nils Schöneberg, Julien Lesgourgues, Michael Walther, Solène Chabanier, and Eric Armengaud, “Hints, neutrino bounds and WDM constraints from SDSS DR14 Lyman- α and Planck full-survey data,” *JCAP* **04**, 038 (2020), [arXiv:1911.09073 \[astro-ph.CO\]](#).
- [22] Alexander Reeves, Laura Herold, Sunny Vagnozzi, Blake D. Sherwin, and Elisa G. M. Ferreira, “Restoring cosmological concordance with early dark energy and massive neutrinos?” *Mon. Not. Roy. Astron. Soc.* **520**, 3688–3695 (2023), [arXiv:2207.01501 \[astro-ph.CO\]](#).
- [23] Gioacchino Ranucci, “The Profile likelihood ratio and the look elsewhere effect in high energy physics,” *Nucl. Instrum. Meth. A* **661**, 77–85 (2012), [arXiv:1201.4604 \[physics.data-an\]](#).
- [24] J. Neyman, “Outline of a Theory of Statistical Estimation Based on the Classical Theory of Probability,” *Phil. Trans. Roy. Soc. Lond. A* **236**, 333–380 (1937).
- [25] Emil Brinch Holm, Andreas Nygaard, Jeppe Dakin, Steen Hannestad, and Thomas Tram, “PROSPECT: A profile likelihood code for frequentist cosmological parameter inference,” (2023), [arXiv:2312.02972 \[astro-ph.CO\]](#).
- [26] Andreas Nygaard, Emil Brinch Holm, Steen Hannestad, and Thomas Tram, “CONNECT: a neural network based framework for emulating cosmological observables and cosmological parameter inference,” *JCAP* **05**, 025 (2023), [arXiv:2205.15726 \[astro-ph.IM\]](#).
- [27] Zack Li *et al.*, “The Atacama Cosmology Telescope: limits on dark matter-baryon interactions from DR4 power spectra,” *JCAP* **02**, 046 (2023), [arXiv:2208.08985 \[astro-ph.CO\]](#).

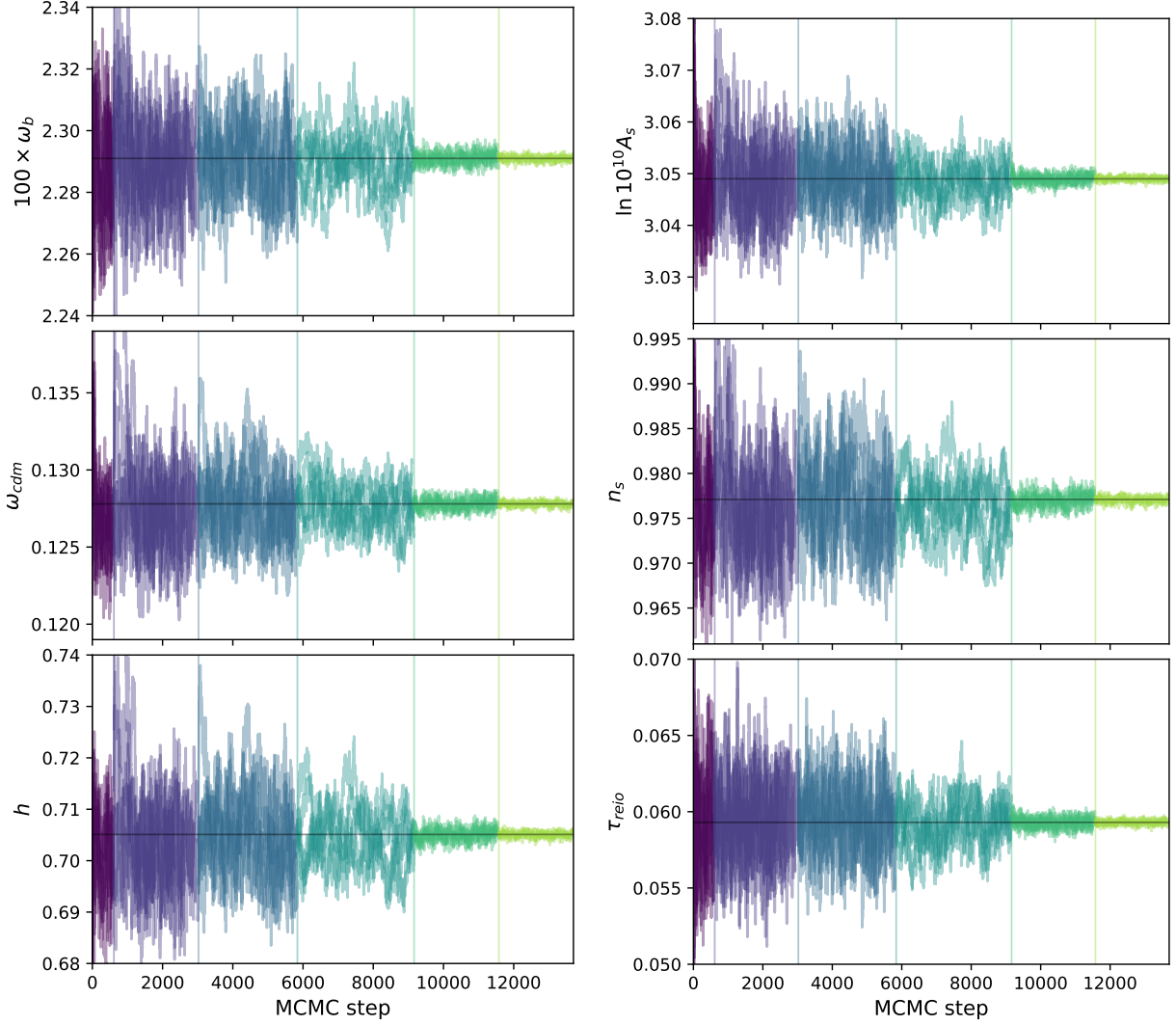


FIG. 10. Convergence of the 6 Λ CDM parameters to the fiducial cosmology in Table I, using Procoli default settings for the global optimization. As before, each step in the SA ladder is differentiated by color and by a vertical line. The horizontal black lines mark the positions of the input fiducial cosmology.

- [28] Emil Brinch Holm, Laura Herold, Steen Hannestad, Andreas Nygaard, and Thomas Tram, “Decaying dark matter with profile likelihoods,” *Phys. Rev. D* **107**, L021303 (2023), [arXiv:2211.01935 \[astro-ph.CO\]](#).
- [29] Benjamin Audren, Julien Lesgourgues, Karim Benabed, and Simon Prunet, “Conservative Constraints on Early Cosmology: an illustration of the Monte Python cosmological parameter inference code,” *JCAP* **1302**, 001 (2013), [arXiv:1210.7183 \[astro-ph.CO\]](#).
- [30] Thejs Brinckmann and Julien Lesgourgues, “MontePython 3: boosted MCMC sampler and other features,” *Phys. Dark Univ.* **24**, 100260 (2019), [arXiv:1804.07261 \[astro-ph.CO\]](#).
- [31] Diego Blas, Julien Lesgourgues, and Thomas Tram, “The Cosmic Linear Anisotropy Solving System (CLASS) II: Approximation schemes,” *JCAP* **07**, 034 (2011), [arXiv:1104.2933 \[astro-ph.CO\]](#).
- [32] Jesus Torrado and Antony Lewis, “Cobaya: Code for Bayesian Analysis of hierarchical physical models,” *JCAP* **05**, 057 (2021), [arXiv:2005.05290 \[astro-ph.IM\]](#).
- [33] Jesús Torrado and Antony Lewis, “Cobaya: Bayesian analysis in cosmology,” Astrophysics Source Code Library, record ascl:1910.019 (2019), [ascl:1910.019](#).
- [34] Cullan Howlett, Antony Lewis, Alex Hall, and Anthony Challinor, “CMB power spectrum parameter degeneracies in the era of precision cosmology,” *JCAP* **04**, 027 (2012), [arXiv:1201.3654 \[astro-ph.CO\]](#).
- [35] Antony Lewis, Anthony Challinor, and Anthony Lasenby, “Efficient computation of CMB anisotropies in closed FRW models,” *Astrophys. J.* **538**, 473–476 (2000), [arXiv:astro-ph/9911177](#).
- [36] Steen Hannestad, “Stochastic optimization methods for extracting cosmological parameters from cosmic microwave background radiation power spectra,” *Phys. Rev. D* **61**, 023002 (2000), [arXiv:astro-ph/9911330](#).
- [37] Nils Schöneberg, Guillermo Franco Abellán, Andrea Pérez Sánchez, Samuel J. Witte, Vivian Poulin, and Julien Lesgourgues, “The H0 Olympics: A fair rank-

- ing of proposed models,” *Phys. Rept.* **984**, 1–55 (2022), [arXiv:2107.10291 \[astro-ph.CO\]](#).
- [38] Samuel Goldstein, J. Colin Hill, Vid Iršič, and Blake D. Sherwin, “Canonical Hubble-Tension-Resolving Early Dark Energy Cosmologies Are Inconsistent with the Lyman- α Forest,” *Phys. Rev. Lett.* **131**, 201001 (2023), [arXiv:2303.00746 \[astro-ph.CO\]](#).
 - [39] Joanna Dunkley, Martin Bucher, Pedro G. Ferreira, Kavilan Moodley, and Constantinos Skordis, “Fast and reliable mcmc for cosmological parameter estimation,” *Mon. Not. Roy. Astron. Soc.* **356**, 925–936 (2005), [arXiv:astro-ph/0405462](#).
 - [40] Hans Dembinski, Piti Ongmongkolkul, Christoph Deil, Henry Schreiner, Matthew Feickert, Chris Burr, Jason Watson, Fabian Rost, Alex Pearce, Lukas Geiger, Ahmed Abdelmotteleb, Aman Desai, Bernhard M. Wiedemann, Christoph Gohlke, Jeremy Sanders, Jonas Drotleff, Jonas Eschle, Ludwig Neste, Marco Edward Gorelli, Max Baak, Michael Eliachevitch, and Omar Zapata, “scikit-hep/iminuit,” (2023).
 - [41] F. James and M. Roos, “Minuit: A System for Function Minimization and Analysis of the Parameter Errors and Correlations,” *Comput. Phys. Commun.* **10**, 343–367 (1975).
 - [42] Antony Lewis, “GetDist: a Python package for analysing Monte Carlo samples,” (2019), [arXiv:1910.13970 \[astro-ph.IM\]](#).
 - [43] Tanvi Karwal and Marc Kamionkowski, “Dark energy at early times, the Hubble parameter, and the string axiverse,” *Phys. Rev. D* **94**, 103523 (2016), [arXiv:1608.01309 \[astro-ph.CO\]](#).
 - [44] Vivian Poulin, Tristan L. Smith, Tanvi Karwal, and Marc Kamionkowski, “Early Dark Energy Can Resolve The Hubble Tension,” *Phys. Rev. Lett.* **122**, 221301 (2019), [arXiv:1811.04083 \[astro-ph.CO\]](#).
 - [45] Vivian Poulin, Tristan L. Smith, Daniel Grin, Tanvi Karwal, and Marc Kamionkowski, “Cosmological implications of ultralight axionlike fields,” *Phys. Rev. D* **98**, 083525 (2018), [arXiv:1806.10608 \[astro-ph.CO\]](#).
 - [46] Vivian Poulin, Tristan L. Smith, and Tanvi Karwal, “The Ups and Downs of Early Dark Energy solutions to the Hubble tension: A review of models, hints and constraints circa 2023,” *Phys. Dark Univ.* **42**, 101348 (2023), [arXiv:2302.09032 \[astro-ph.CO\]](#).
 - [47] Marc Kamionkowski and Adam G. Riess, “The Hubble Tension and Early Dark Energy,” *Ann. Rev. Nucl. Part. Sci.* **73**, 153–180 (2023), [arXiv:2211.04492 \[astro-ph.CO\]](#).
 - [48] Adam G. Riess, Louise Breuval, Wenlong Yuan, Stefano Casertano, Lucas M. Macri, J. Bradley Bowers, Dan Scolnic, Tristan Cantat-Gaudin, Richard I. Anderson, and Mauricio Cruz Reyes, “Cluster Cepheids with High Precision Gaia Parallaxes, Low Zero-point Uncertainties, and Hubble Space Telescope Photometry,” *Astrophys. J.* **938**, 36 (2022), [arXiv:2208.01045 \[astro-ph.CO\]](#).
 - [49] Jose Luis Bernal, Licia Verde, and Adam G. Riess, “The trouble with H_0 ,” *JCAP* **10**, 019 (2016), [arXiv:1607.05617 \[astro-ph.CO\]](#).
 - [50] Kevin Aylor, MacKenzie Joy, Lloyd Knox, Marius Millea, Srinivasan Raghunathan, and W. L. Kimmy Wu, “Sounds Discordant: Classical Distance Ladder & Λ CDM-based Determinations of the Cosmological Sound Horizon,” *Astrophys. J.* **874**, 4 (2019), [arXiv:1811.00537 \[astro-ph.CO\]](#).
 - [51] Lloyd Knox and Marius Millea, “Hubble constant hunter’s guide,” *Phys. Rev. D* **101**, 043533 (2020), [arXiv:1908.03663 \[astro-ph.CO\]](#).
 - [52] Meng-Xiang Lin, Giampaolo Benevento, Wayne Hu, and Marco Raveri, “Acoustic Dark Energy: Potential Conversion of the Hubble Tension,” *Phys. Rev. D* **100**, 063542 (2019), [arXiv:1905.12618 \[astro-ph.CO\]](#).
 - [53] Prateek Agrawal, Francis-Yan Cyr-Racine, David Pinner, and Lisa Randall, “Rock ‘n’ roll solutions to the Hubble tension,” *Phys. Dark Univ.* **42**, 101347 (2023), [arXiv:1904.01016 \[astro-ph.CO\]](#).
 - [54] Florian Niedermann and Martin S. Sloth, “New early dark energy,” *Phys. Rev. D* **103**, L041303 (2021), [arXiv:1910.10739 \[astro-ph.CO\]](#).
 - [55] Tanvi Karwal, Marco Raveri, Bhuvnesh Jain, Justin Khoury, and Mark Trodden, “Chameleon early dark energy and the Hubble tension,” *Phys. Rev. D* **105**, 063535 (2022), [arXiv:2106.13290 \[astro-ph.CO\]](#).
 - [56] Kim V. Berghaus and Tanvi Karwal, “Thermal Friction as a Solution to the Hubble Tension,” *Phys. Rev. D* **101**, 083537 (2020), [arXiv:1911.06281 \[astro-ph.CO\]](#).
 - [57] Kim V. Berghaus and Tanvi Karwal, “Thermal friction as a solution to the Hubble and large-scale structure tensions,” *Phys. Rev. D* **107**, 103515 (2023), [arXiv:2204.09133 \[astro-ph.CO\]](#).
 - [58] Evan McDonough, Meng-Xiang Lin, J. Colin Hill, Wayne Hu, and Shengjia Zhou, “Early dark sector, the Hubble tension, and the swampland,” *Phys. Rev. D* **106**, 043525 (2022), [arXiv:2112.09128 \[astro-ph.CO\]](#).
 - [59] Lucy Brissenden, Konstantinos Dimopoulos, and Samuel Sánchez López, “Non-oscillating early dark energy and quintessence from α -attractors,” *Astropart. Phys.* **157**, 102925 (2024), [arXiv:2301.03572 \[astro-ph.CO\]](#).
 - [60] Matteo Braglia, Mario Ballardini, Fabio Finelli, and Kazuya Koyama, “Early modified gravity in light of the H_0 tension and LSS data,” *Phys. Rev. D* **103**, 043528 (2021), [arXiv:2011.12934 \[astro-ph.CO\]](#).
 - [61] Mark Gonzalez, Mark P. Hertzberg, and Fabrizio Rompineve, “Ultralight Scalar Decay and the Hubble Tension,” *JCAP* **10**, 028 (2020), [arXiv:2006.13959 \[astro-ph.CO\]](#).
 - [62] Jeremy Sakstein and Mark Trodden, “Early Dark Energy from Massive Neutrinos as a Natural Resolution of the Hubble Tension,” *Phys. Rev. Lett.* **124**, 161301 (2020), [arXiv:1911.11760 \[astro-ph.CO\]](#).
 - [63] N. Aghanim *et al.* (Planck), “Planck 2018 results. V. CMB power spectra and likelihoods,” *Astron. Astrophys.* **641**, A5 (2020), [arXiv:1907.12875 \[astro-ph.CO\]](#).
 - [64] N. Aghanim *et al.* (Planck), “Planck 2018 results. VIII. Gravitational lensing,” *Astron. Astrophys.* **641**, A8 (2020), [arXiv:1807.06210 \[astro-ph.CO\]](#).
 - [65] Florian Beutler, Chris Blake, Matthew Colless, D. Heath Jones, Lister Staveley-Smith, Lachlan Campbell, Quentin Parker, Will Saunders, and Fred Watson, “The 6dF Galaxy Survey: Baryon Acoustic Oscillations and the Local Hubble Constant,” *Mon. Not. Roy. Astron. Soc.* **416**, 3017–3032 (2011), [arXiv:1106.3366 \[astro-ph.CO\]](#).
 - [66] Ashley J. Ross, Lado Samushia, Cullan Howlett, Will J. Percival, Angela Burden, and Marc Manera, “The clustering of the SDSS DR7 main Galaxy sample – I. A 4 per cent distance measure at $z = 0.15$,” *Mon. Not. Roy. Astron. Soc.* **449**, 835–847 (2015), [arXiv:1409.3242 \[astro-ph.CO\]](#).
 - [67] Adam G. Riess *et al.*, “A Comprehensive Measurement

of the Local Value of the Hubble Constant with 1 km s^{-1}
 Mpc^{-1} Uncertainty from the Hubble Space Telescope and

the SH0ES Team,” *Astrophys. J. Lett.* **934**, L7 (2022),
[arXiv:2112.04510 \[astro-ph.CO\]](#).